

Combination of advanced 2D PIV and Stereo Technique

**Sara Nauri, Mathieu Legrand, Antonio Lecuona, Pedro A. Rodríguez,
José Nogueira**

Department of Thermal and Fluids Engineering, Universidad Carlos III, Madrid, Spain, goriba@ing.uc3m.es

Abstract Particle Image Velocimetry with Local Field Correction (LFC-PIV) has been tested in the past to obtain two components of the velocity in a two dimensional domain (2D2C). When compared with conventional correlation based algorithms, this advanced technique has showed improvements in three important aspects: robustness, resolution and ability to cope with large displacement gradients.

A further step in the development of PIV algorithms consists in the combination of LFC with the Stereo technique, able to obtain three components of the velocity (2D3C PIV). To successfully apply stereoscopy, the laser sheet width is usually larger than in 2C velocimetry, in order to acquire the out of plane displacement of the particles. This peculiarity can make questionable the need for improved spatial resolution. In particular, if some factors concur the measurement of small scale features of the velocity along the laser sheet can be spoiled by the velocity variations across it, caused by the flow structures.

Being the spatial resolution capabilities of LFC its main advantage, this paper focuses in establishing if there are advantages left for LFC-PIV in situations where only large scale features are of interest, thus making it difficult for this technique to show its attractiveness. The remaining benefits still to be analyzed are the robustness and the ability to cope with large displacement gradients. For both aspects, the performances of 2D3C-LFC-PIV are explored. These performances are characterized and compared with conventional and other advanced algorithms, when applied to synthetic PIV images. In addition, the coherence between these results and those coming from experimental PIV images is presented and discussed.

1. Introduction

Contemporary Particle Image Velocimetry (PIV) is now applied with confidence in industrial facilities such as large wind tunnels. Many research and development programs have obtained benefits out of this measurement technique (CoJeN, Heliflow, Apian, C-wake in Europe, among others). Even though this indicates a broad application of PIV in industrial scale setups, a significant effort is still dedicated to increase its applicability, capabilities and accuracy. This includes the development of new algorithms and techniques. Among them, two branches are of interest for this work:

- The conventionally named “advanced algorithms” that deal with the improvement of two-dimensional PIV, which is designed to measure two-components of the velocity (2D-2C PIV). The main objectives of these algorithms are the increase of the spatial resolution, the ability to cope with large displacement gradients and an enhancement of the robustness (i.e. capability to avoid outliers) when dealing with reduced signal to noise ratios.
- The Stereo PIV technique, which combines the information of different planar views of the field under study to obtain the three components of the velocity (2D-3C PIV).

The combination of these two branches is a domain that has to be fully explored. For particular flow conditions and experimental setups, some of the advantages of the advanced PIV algorithms might not be useful when using this combination. An example of this can illustrate the point: Lets consider a flow of homogeneous turbulence and laser sheet width thicker than the length corresponding to 30 pixels (when considering a certain magnification defined at the image sensor).

In such a scenario, the presence of vortex of scales smaller than ~ 30 pixels would generate velocity gradients in the out of plane direction that contemporary Stereoscopic PIV techniques would not be able to fully discriminate from gradients along the plane. The consequence for such an experimental setup is that only scales significantly larger could be properly assessed in the measurement. In this example the improved resolution of an advanced algorithm like the local field correction PIV (LFC-PIV) (Nogueira *et al.* 2001), that is able to extract in-plane flow features in the order of 25 pixels size with 10% errors (Lecuona *et al.* 2004), would be useless. This is mainly due to the out-of-plane overlapping of information.

After the previous considerations, some insight in the other two main advantages of LFC-PIV (robustness and the ability to cope with large displacement gradients) has to be performed. Even considering the case of flow features with large characteristic lengths, the advantages on these two other metrological aspects may be still available in a Stereo configuration and be useful for the researcher:

- The ability to cope with large particle displacement gradients, among other possibilities, allows increasing the time between images (Δt). This usually reduces the effect of subpixel accuracy limitations (better measurements with the same subpixel accuracy).
- The enhancement of robustness has a particular interesting role when dealing with the out-of-plane loss of particle pairs, very frequent in 3D flows. Again, ability to cope with large percentages of particle image losses allows increasing Δt .

Knowing the limits on the capability to cope with large gradients and out-of-plane loss of particles in 2D3C LFC-PIV seems interesting. It allows designing experiments or deciding on the need to introduce advanced algorithms in a Stereo PIV measurement. In this paper these limits are explored using synthetic images (Sections 3 and 4) and real images (Section 5).

2. Algorithms under test and Synthetic images

Three types of algorithms have been tested using these images:

- (i) Conventional PIV algorithms applied in a Stereo configuration. They consist in a single pass processing of an interrogation window of 64 pixels size.
- (ii) Stereo LFC-PIV which, apart from image distortion, adds the benefits of a particular weighting function (Nogueira *et al.* 2001). As a result, it does neither need smoothing of the velocity field in the iterative process nor reduction of the interrogation window size of 64 pixels.
- (iii) Multigrid PIV with image distortion applied in a Stereo configuration. In this case, smoothing is needed to avoid the growth of the unstable wavelengths (Nogueira *et al.* 2002, Scarano *et al.* 2004, among others). Different ways of smoothing may be used. In this work it consists in a moving average of the vector field for all the iterations except the last one. The particular smoothing algorithm is not considered to be too relevant, as only large flow scales are analyzed. The initial window size for this algorithm has been set to 64 pixels in order to test its robustness in a common base with the conventional and LFC algorithms.

In agreement with the aim of the work, it should be noted that the spatial resolution of the three methods is significantly smaller than the characteristic spatial wavelengths of the flow features analyzed in this paper (larger than 300 pixels).

Although tests on real images are the final objective, the preliminary use of synthetic images to test the performance of a PIV algorithm has become usual (Westerweel *et al.* 1997, Fincham and Spedding, 1997, Scarano and Riethmuler, 2000, among others). For this work, the synthetic image generator used by the authors in the past (Lecuona *et al.* 2004, Nogueira *et al.* 2005) has been improved to reproduce the frames corresponding to a desired stereo configuration. The stereo configuration chosen to generate the synthetic images here described and used in Sections 3 and 4

matches the ones of the real setup used in Section 5. The cameras are in a forward-forward scattering Willert configuration (Willert, 1997). The angle between the laser sheet and the cameras is 45 degrees and the magnification at the center of the image is $70 \mu\text{m} / \text{pixel}$.

Synthetic images were purposely designed to test the ability to cope with large displacement gradients and the out-of-plane loss of particles. They contain no noise except for the spatial discretisation of the simulated image sensor and the usual effective 8-bit gray level sampling. The average distance between the randomly located particle images is small, $\delta = 2$ pixels, i.e. $4/(\pi\delta^2) \approx 0.3$ ppp (particles per pixel) at the center of the image and varies accordingly to the 3D perspective. The e^{-2} diameter of all the Gaussian particle images is $d = 2$ pixels. This diameter is considered as a diffraction characteristic feature of the lenses and thus does not vary with the perspective. No vignetting is considered. The Gaussian shape of the particle images is integrated with unity fill factor over each square pixel surface (Westerweel 1998). A top-hat constant intensity profile was selected for the light sheet, so that each particle can equally contribute to the correlation. Where particles overlap, the corresponding intensities were added. The associated particle surface density is on the edge where speckle pattern may start to appear, but this phenomenon will not be taken into account in this paper. The underlying principle behind the high-density chosen is to reduce the error due to the sampling of the flow field and consequently more clearly reveal the effect of the parameters under study. On the other hand, the resulting images look very similar to real ones obtained in large wind tunnel careful experiments, being the particle surface density similar. The grey level saturation resulted to be statistically insignificant.

The test displacement field implemented in these images corresponds to a modified Rankine vortex. The velocity flow field in each image follows the expression:

$$v_\theta = \frac{2U_0 (r/R_0)}{1 + (r/R_0)^2}; \quad v_r = 0 \quad (1)$$

Where U_0 is the maximum tangential velocity, located at the vortex radius $r = R_0$. The total vortex circulation is $\Gamma = 4\pi R_0 U_0$. The parameters selected in the analysis of Section 3 to define the vortex are the Radius R_0 , and the vorticity (curl of the velocity), a basic flow magnitude for viscous structures. At the center of the vortex, the peak vorticity, ω_p , corresponds to:

$$\omega_p = 4U_0/R_0 \quad (2)$$

It diminishes to quickly reach $\omega_p/4$ at a distance R_0 of the center of the vortex

3. Vorticity tests

The response of conventional PIV to vortexes of different sizes and its comparison with LFC-PIV performance can be found in Lecuona *et al.* (2004). In that reference, an extensive study is reported on the effect of group locking. This effect explains the reason why the error of conventional PIV at obtaining the peak vorticity does not vanish as the scale of the vortex to evaluate grows. Moreover, this effect is also present when the peak vorticity is reduced to $\omega_p < 0.06 \Delta t^{-1}$ as prescribed by Keane and Adrian (1993). In this scenario (Lecuona *et al.* 2004), 2D2C LFC-PIV performed with no group locking and was able to describe peak vorticities up to $\omega_p < 1.2 \Delta t^{-1}$, clearly higher than those of conventional PIV.

In this section the previously commented algorithms are applied over large vortexes in a Stereo configuration (2D3C). This allows checking the benefits of the ability to cope with large displacements gradients in the two aspects previously mentioned:

- A reduced uncertainty of Stereo LFC-PIV measurements due to its low susceptibility to group-locking.
- The capability of Stereo LFC-PIV to deal with larger displacement gradients than a conventional correlation Stereo PIV, thus allowing for the selection of larger Δt in the experiments where it is used.

For these tests, a set of synthetic images of a vortex have been generated with different peak vorticities. The results for a conventional Stereo PIV, multigrid Stereo PIV enhanced with image distortion and Stereo LFC-PIV are presented in figure 1.

In this figure, the errors from PIV data have been evaluated by calculating a normalized error value. It corresponds to the root mean square of the error divided by the root mean square of the value of the vectors to analyze $[\text{rms}(e)/\text{rms}(s)]$ in the area where $r/R_0 < 2$. R_0 has been fixed as 96 pixels for all the cases.

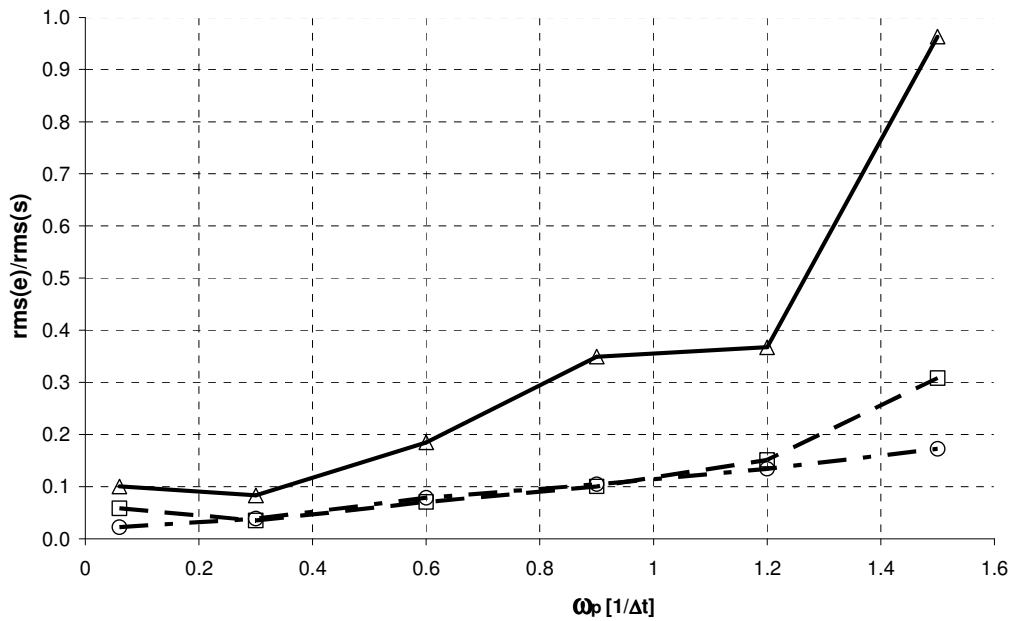


Figure 1. Comparison of the normalized error for Stereo setups of: conventional Stereo PIV (triangles), Multigrid Stereo PIV enhanced with image distortion (squares) and Stereo LFC-PIV (circles) on a vortex flow for different peak vorticity values.

For the implementation of the conventional Stereo PIV algorithm, the search of the correlation peak has been restricted to the range of velocities present in each evaluation. This way a the incidence of outliers is reduced. In this frame, measurements with normalized error below 20% can be obtained for $\omega_p < 0.6 \Delta t^{-1}$. For larger vorticities, image distortion algorithms are needed. Once image distortion is used, the lack of smoothing of Stereo LFC-PIV allows it to show improvement only for $\omega_p < 0.2 \Delta t^{-1}$. and $\omega_p > 1 \Delta t^{-1}$. Moreover, the smoothing used by the multigrid scheme improves the results in a small percentage for the interval $0.2 \Delta t^{-1} < \omega_p < 1 \Delta t^{-1}$. This better result for a smoothing algorithm that discards the small details is coherent with the fact that this evaluation is done in absence of small scale features. Above $\omega_p \sim 1.5 \Delta t^{-1}$ (which corresponds to a rotation of $\sim 43^\circ$) the path of the tracer particle has a noticeable difference with the straight line segment between initial and final locations. In consequence, this region has not been further studied.

4. Out-of-plane displacement tests

As commented before, one of the problems when increasing the time between light pulses is the increment of out-of-plane loss of particle pairs. It is of interest to evaluate how much of this out-of-plane loss is tolerable by an advanced algorithm in a Stereo configuration. For this evaluation, synthetic images that correspond to the vortex used in the previous section with $\omega_p < 0.06 \Delta t^{-1}$, with different out-of-plane velocities were generated. Again, these images were analyzed by the previous three methods. The $\text{rms}(e)/\text{rms}(s)$ for $r/R_0 < 2$ has been calculated taking into account only the in-plane components of the velocity as the out-of-plane component was just a uniform translation. The results are presented in figure 2.

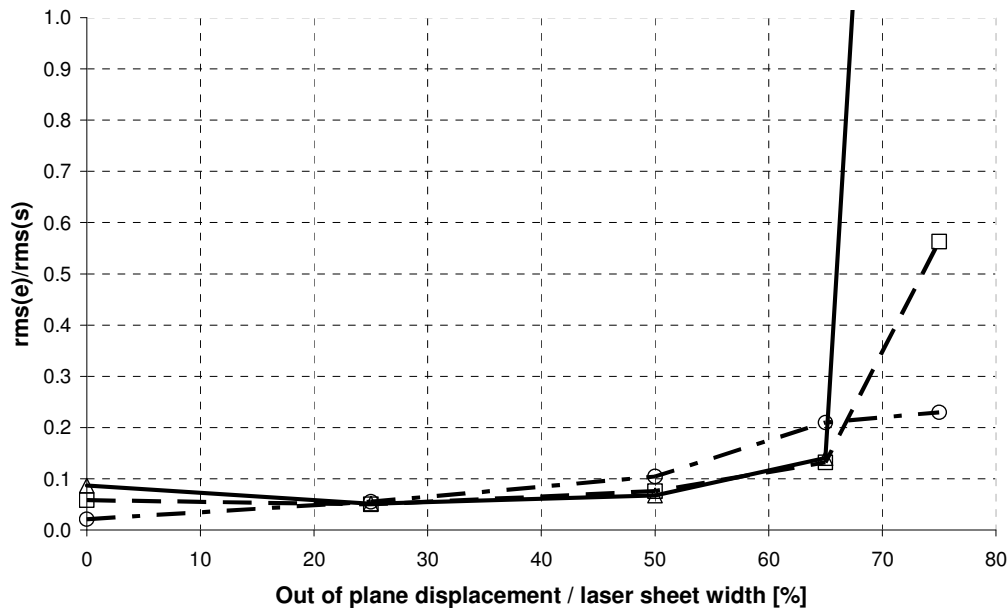


Figure 2. Comparison of the normalized error for Stereo setups as a function of the out-of-plane displacement produced by conventional Stereo PIV (triangles), Multigrid Stereo PIV enhanced with image distortion (squares) and Stereo LFC-PIV (circles).

Although robustness is a difficult to quantify characteristic, qualitative comparisons are possible. Figure 2 shows that conventional Stereo PIV (with restricted correlation peak search) and the advanced iterative methods perform with an acceptable error for out-of-plane displacements up to 65% of the laser sheet width (65% of the particles at each PIV image do not have the corresponding couple in the other PIV image), without additional sources of error. Again smoothing of the Multigrid PIV with image distortion reduces the error coming from iterations an additional small percentage in respect to LFC-PIV, attributing this to the absence of small scale flow features. It is relevant to notice that weighting of the interrogation window of the LFC algorithm does not reduce its robustness with respect to the 64 pixels interrogation window of the multigrid approach. On the contrary, it performs better for out of plane displacements of 75% of the laser sheet width.

5. Vorticity combined with out-of-plane displacement tests

One last test has been run on synthetic images, now combining significant vorticity and out of plane velocity (50% of the laser sheet width).

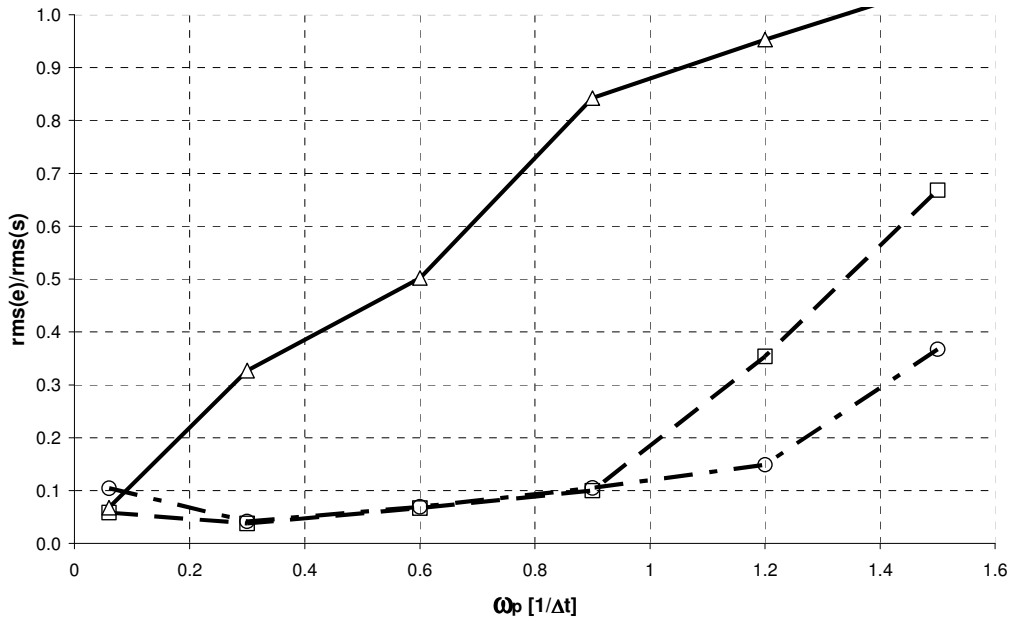


Figure 3. Comparison of the normalized error for Stereo setups as a function of the peak vorticity for a significant out-of-plane displacement (50% of the laser sheet width). Conventional Stereo PIV (triangles), Multigrid Stereo PIV enhanced with image distortion (squares) and Stereo LFC-PIV (circles).

The results for the three methods under study are depicted in figure 3. For the case of advanced algorithms, it is evident that even with a total absence of small scales features, the use of the Stereo LFC-PIV combination offers an improved robustness when dealing with significant velocity gradients. It is important to notice that when evaluating a certain case, for example $\omega_p = 1.2 \Delta t^{-1}$, the vorticity in most of the $r/R_0 < 2$ area is significantly smaller ($\omega = 0.4 \Delta t^{-1}$ at $r = R_0$)

To offer a visual idea of the amount of error depicted in the plots in figures 1, 2 and 3, the vector maps, corresponding to $\omega_p = 1.2 \Delta t^{-1}$ in figure 3, have been plotted in figure 4 for both evaluation methods. The magnification corresponds to $M = 16$ pixels/mm. Although it has no small-scale features, the combination of $\omega_p = 1.2 \Delta t^{-1}$ and out-of-plane displacement $\sim 50\%$ (~ 16 pixels) makes it a difficult measurement.

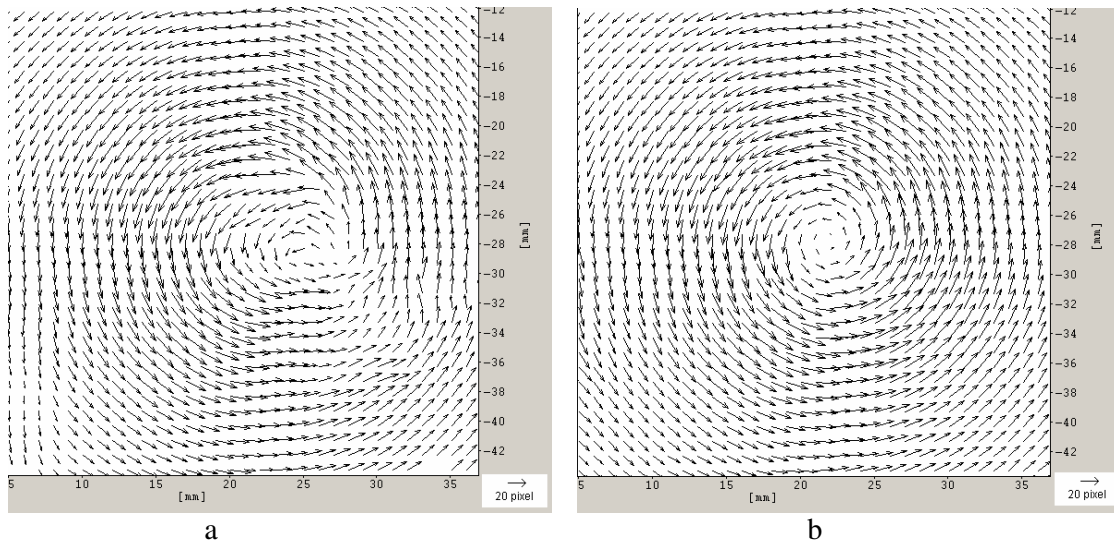


Figure 4. Vector plots of the in-plane velocity showing presence of errors for Stereo evaluations of the vortex flow with out-of-plane displacement. a) Measurement from Multigrid Stereo PIV enhanced with image distortion. b) Stereo LFC-PIV measurement.

6. Application to real images

The previous study has been performed on synthetic PIV images. These images act as a powerful tool that allows exposing particular details and reveal the underlying mechanisms. Nevertheless, the genuine objective of the work here reported is real images. Even though the detailed flow field is unknown, thus impeding to offer a measurement error figure, tests are customary for checking the coherence between the results found with synthetic images and those with real ones.

In this section, tests on real images are designed to study the mentioned coherence with the particular results obtained on the synthetic images from the previous sections. The tests show the suitability of the Stereo-LFC-PIV method. Actually, this is the first time that such a combination has been used, up to the knowledge of the authors.

In a similar way than in the synthetic image cases, special attention is paid to large displacement gradients and out-of-plane displacements. With these aims, Stereo PIV images have been obtained in a small open jet facility. The working fluid is air at atmospheric conditions. The diameter of the jet nozzle is 50 mm and the flow was set to an average of ~ 2 m/s. The Reynolds number based on the jet nozzle diameter is $Re_D = 6,600$. It has been seeded with food-grade glycol droplets of $\sim 1 \mu\text{m}$ in diameter. This fluid was chosen because of its non-toxicity and the fact that it evaporates after long periods leaving the laboratory free of residues. The seeding device consisted in several Laskin-like nozzles of known characteristics (Kähler, Sammler and Kompenhans, 2001). The images were taken at 4 diameters downstream the exit nozzle. The magnification in the center of the planes corresponds to 14 to 16 pixels/mm, depending on the image. The Stereo configuration corresponds to that of the synthetic images (forward-forward scattering Willert configuration at 45 degrees of the laser sheet). The cameras sensors consist of 2k by 2k pixels with 12 bits sampling. The laser corresponds to a double head NdYag shooting 380 mJ per pulse. Two different positions were studied:

- To check the cases with no out-of-plane displacement, the laser sheet was located in a meridional plane of the nozzle. Figure 5a shows an example of the images obtained in this position.

- For cases with out-of-plane displacement, the laser sheet was located parallel to the previous position but displaced 20 mm off-axis. Figure 5b shows an example of the images obtained at this position. The vortexes are intersected by the laser sheet at a non-perpendicular angle to their axis of rotation. As a result, their rotation generates out-of-plane components of the displacement in addition to the in-plane components

Images in figure 5 correspond to low and inhomogeneous seeding in the outside of the jet. These seeding inhomogeneities aid the visualization of the flow.

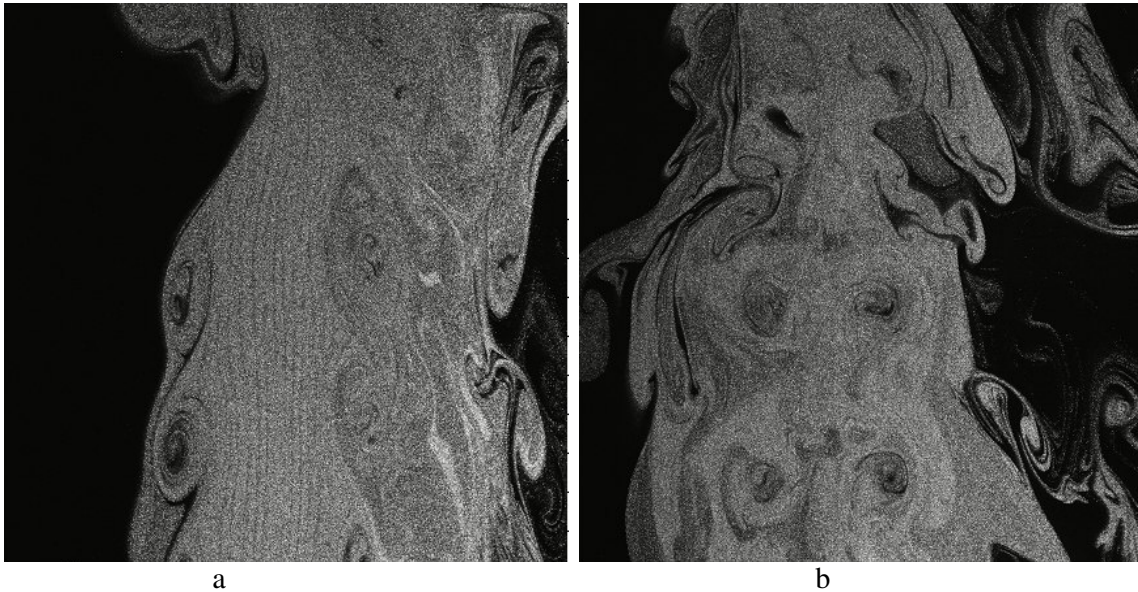


Figure 5. Example of images of the jet under study. a) Laser sheet located at a meridional plane of the round nozzle. b) Laser sheet parallel to a meridional plane but displaced 20 mm towards the observer.

Examples of Stereo measurements in both locations are given in figures 6 and 7. Please, note that only a small portions of ~ 400 by 400 pixels are presented out of the $2k$ by $2k$ images. These portions are selected out of zones where there are no seeding inhomogeneity difficulties for PIV. The coherence with the synthetic images measurements cases is clear. Outliers are more evident in the measurement from Multigrid Stereo PIV enhanced with image distortion than in the Stereo LFC-PIV one.

Measurements of the laser sheet revealed an almost Gaussian profile with an e^{-2} width of ~ 2 mm. In the case of figure 7, the magnification corresponds to 16 pixels/mm. In consequence, the out-of-plane displacement is in the order of 0.5 mm (25% of the plane width). The presence of outliers for this out-of-plane value can be related to the fact that in real images other sources of error makes more difficult for any algorithm to perform satisfactorily.

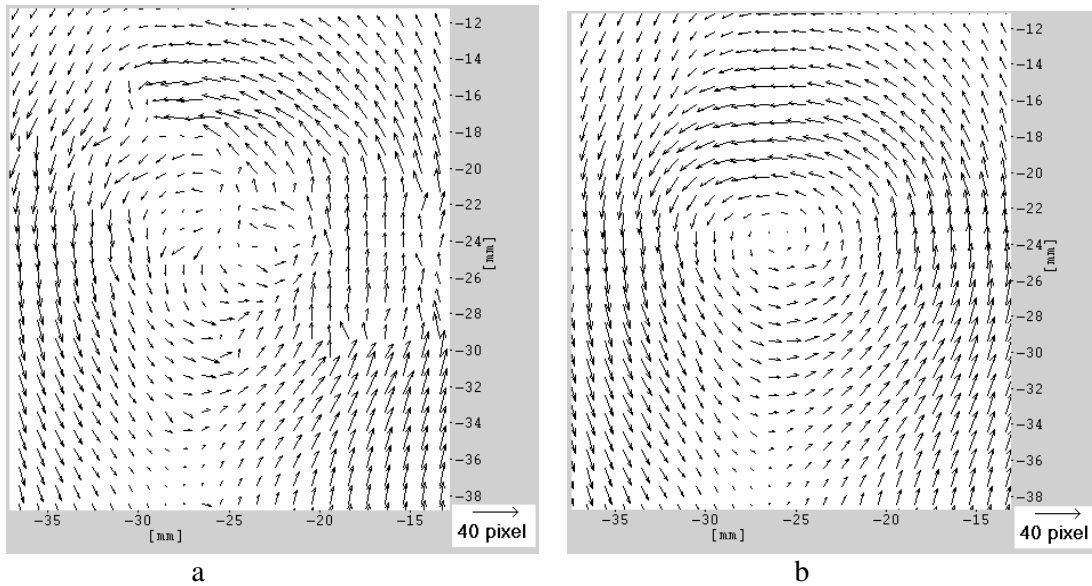


Figure 6. Vector plots for Stereo evaluations of a vortex from figure 5a. The peak vorticity corresponds to $\omega_p \sim 1.2 \Delta t^{-1}$ a) measurement with Multigrid Stereo PIV enhanced with image distortion. b) Stereo LFC-PIV measurement.

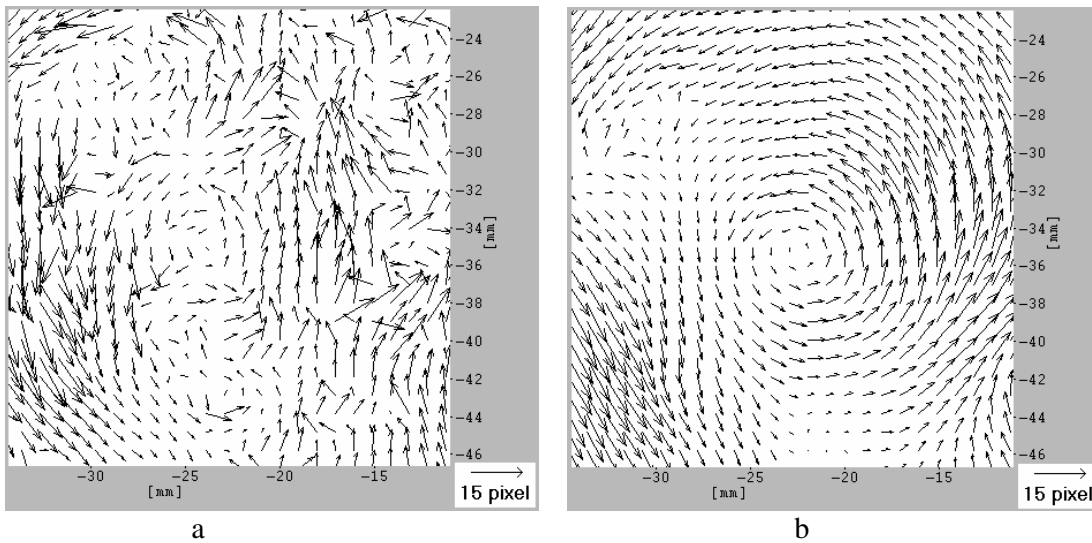


Figure 7. Vector plots for Stereo evaluations of a vortex from figure 5b. The peak vorticity corresponds to $\omega_p \sim 0.25 \Delta t^{-1}$. The out-of-plane component varies from 10.8 pixels in the upper side to -8.5 pixels in the lower part. a) measurement with Multigrid Stereo PIV enhanced with image distortion. b) Stereo LFC-PIV measurement.

7. Conclusions

This paper offers results of the first implementation of LFC-PIV in a Stereo setup. Due to the usually large width of the laser sheet in Stereo configurations, a particular case in which the high-resolution capability of this technique is not needed has been selected for the tests, as small wavelengths are not present. This allows evaluating other advantages of the LFC-PIV algorithms.

The results show that the ability to cope with large gradients can help in this kind of setups allowing to increase Δt in vortex flows, thus increasing the velocity measurement dynamic range. Correct measurements have been achieved with vorticities as large as $\omega_p \sim 1.5 \Delta t^{-1}$. This corresponds to a rotation of $\sim 43^\circ$; which is ~ 20 times the maximum vorticity prescribed by Kean and Adrian (1993) for a conventional correlation PIV.

It is relevant to notice that the weighting of the interrogation window of the Stereo-LFC algorithm does not reduce its robustness when compared with the same window size for a Multigrid based Stereo.

The robustness of the algorithm also allows managing larger out-of-plane loss of particles. The tests in this work indicate that Stereo-LFC-PIV can tolerate out-of-plane displacements of 25% of the plane width in real images.

These ranges of values that Stereo-LFC-PIV is able to endure have been characterized in synthetic images, so that no additional sources of error were considered. In addition, tests on real PIV images have shown coherence with these results. These figures increase the possibilities in the selection of larger Δt for a certain experiment, which allows for a better description of small displacements in different parts of the flow field.

One last conclusion is that Stereo-LFC-PIV, similarly to the 2D2C implementation, shows no group locking in its implementation. This allows for more accurate vorticity results even when dealing with low vorticity values.

Acknowledgements

This work has been partially funded by the COJEN European project, Specific Targeted RESEARCH Project EU Contract No. AST3-CT-2003-502790; the Spanish Research Agency grant DPI2002-02453 "Técnicas avanzadas de Velocimetría por Imagen de Partículas (PIV) Aplicadas a Flujos de Interés Industrial" and under the EUROPIV 2 European project (CONTRACT N°: GRD1-1999-10835) and its associated DPI-2000-1839-CE cofunding by the Spanish Research Agency.

References

- Acosta A; Lecuona A; Nogueira J; Ruiz-Rivas U (2002). "Adaptive Linear Filters for PIV Data Derivatives". *11th Int. Symp. on Applications of Laser Techniques to Fluid Mechanics*. Lisbon, Portugal.
- Kean RD; Adrian RJ (1993) "Theory of cross-correlation analysis of PIV images". *Flow Visualization and Image Analysis*. Kluwer Academic Publishers, The Netherlands. pp: 1-25.
- Fincham AM and Spedding GR (1997) "Low-cost, high resolution DPIV for measurement in turbulent fluid flows". *Exp. in Fluids* 23: pp 449-462.
- Kähler CJ; Sammler BS and Kompenhans JK (2001) "Generation and control of particle size distributions for optical velocity measurement techniques in fluid mechanics". 4th Int. Symp. on PIV, Göttingen.
- Lecuona A; Nogueira J; Rodríguez PA (1998) "Flowfield vorticity calculation using PIV data" *Journal of Visualization*, 1 pp 183-193.
- Lecuona A, Nogueira J, Rodríguez P A and Acosta, A (2004) "PIV Evaluation Algorithms for Industrial Applications". *Meas. Sci. Technol.* 12: 1911-1921.
- Nogueira J, Lecuona A Ruiz-Rivas and Rodríguez P A (2002) "Analysis and alternatives in two-dimensional multigrid particle image velocimetry methods: application of a dedicated weighting function and symmetric direct correlation", *Meas. Sci. Technol.*, 13: pp. 963-974.

- Nogueira J; Lecuona A; Rodríguez PA (2001) "Local field correction PIV, implemented by means of simple algorithms, and multigrid versions". *Meas. Sci. Technol.* **12**: 1911-1921.
- Nogueira J, Lecuona A, Rodríguez PA, Alfaro JA and Acosta, A (2004) "Limits on the resolution of correlation PIV iterative methods. Practical implementation and design of weighting functions". *Experiments in fluids*. 38 (in press).
- Scarano F; Riethmuller M L (2000) "Advances in iterative multigrid PIV image processing". *Exp. Fluids*. 29/7: S51-S60.
- Scarano F (2004) "Super-resolution particle image velocimetry interrogation approach by means of velocity second derivatives correlation". *Meas. Sci. Technol.*, 15: pp. 475-486.
- Westerweel J (1998) "Effect of sensor geometry on the performance of PIV". *9th Int. Symp. on Applications of Laser Techniques to Fluid Mechanics*. Instituto Superior Técnico, Lisbon, Portugal.
- Westerweel J; Dabiri D; Gharib M (1997) "The effect of a discrete window offset on the accuracy of cross-correlation analysis of digital PIV recordings". *Exp. in Fluids* **23**: pp 20-28.
- Willert C (1997) "Stereoscopic digital particle image velocimetry for applications in wind túnel flows". *Meas. Sci. Technol.* **8**: 1465-1479